SIMULTANEOUS MEASUREMENTS OF ENERGY AND TEMPERATURE DISSIPATION RATES IN THE FAR FIELD OF A CYLINDER WAKE

Zhiyong Hao, Tongming Zhou and Leok Poh Chua
School of Mechanical and Production Engineering
Nanyang Technological University, Singapore 639798
haozhiyong@pmail.ntu.edu.sg, mtmzhou@ntu.edu.sg, mlpchua@ntu.edu.sg

Yi Tsann Jiang
DSO National Laboratories
20 Science Park Drive, Singapore 118230
jyitsann@dso.org.sg

ABSTRACT

Simultaneous approximations to energy and temperature dissipation rates, denoted as ε_{ap} and χ_{ap}, are obtained using a probe consisting of four hot wires and a pair of parallel cold wires. The performance of the probe in measuring velocity and temperature derivatives and vorticity has been checked satisfactorily by comparing with isotropic calculations. Local isotropy of small-scale turbulent structures is checked. The differences between the present approximations of the two dissipation rates and those obtained by using isotropic relations are also discussed in terms of both their corresponding spectra and the correlation coefficients with respect to different longitudinal separations r. The correlations between the two dissipation fields and the enstrophy are also examined. Whereas ε_{ap} is strongly correlated with ω_3^2, the correlation between ω_3^2 and χ_{ap} is small.

INTRODUCTION

The turbulent energy dissipation rate $\varepsilon(\equiv 2\nu s_{ij}s_{ij})$, the temperature dissipation rate $\chi(\equiv \kappa\theta_{,i}\theta_{,i})$ and the enstrophy $\omega^2(\equiv \omega_i\omega_i)$ are important characteristics of the small-scale properties of turbulence, where $s_{ij}=(u_{i,j}+u_{j,i})/2$ is the rate of strain; ν is the kinematic viscosity and $u_{i,j}\equiv \partial u_i/\partial x_j$; κ is the thermal diffusivity of the fluid, $\theta_{,i}\equiv \partial\theta/\partial x_i$ and ω_i (i = 1,2,3) is the vorticity component. For example, the combination with some power of ε_r and χ_r, the locally averaged values of ε and χ, features in the refined similarity hypothesis for passive scalars (RSHP) (Stolovitzky et al. 1995). The RSHP states that the nth-order moment of the temperature increment $\delta\theta=\theta(x_1+r)-\theta(x_1)$ can be expressed as

$$<(\delta\theta)^n> \sim < \chi_r^{n/2}\varepsilon_r^{-n/6} > r^{n/3} \sim r^{\zeta_\theta(n)} \qquad (1)$$

when the separation r is in the inertial range, i.e. $\eta << r << L_s$, where L_s is the integral length scale and $\zeta_\theta(n)$ is the scaling exponent of $<(\delta\theta)^n>$. Van Atta (1971) assumed that the probability density functions (pdfs) of ε_r and χ_r for the inertial range scales are lognormally distributed and their joint pdf is bivariate lognormal with a correlation coefficient $\rho_{\alpha,\beta}$ defined as

$$\rho_{\alpha,\beta}=\frac{<(\alpha-<\alpha>)(\beta-<\beta>)}{\sigma_\alpha\sigma_\beta} \qquad (2)$$

where α and β represent $\ln\varepsilon_r$ and $\ln\chi_r$ respectively, σ_α and σ_β are the standard deviations of α and β. Therefore, the small-scale scalar characteristics are influenced not only by ε and χ but also by their correlations. The correlation between ε_r and χ_r is important in quantifying $<(\delta\theta)^n>$ and perhaps in a more physical sense, ascertaining the interdependence between the two dissipative fields through their relation to the vortical structure of the flow.

Measurements of either the energy dissipation rate ε or the temperature dissipation rate χ have been made by a number of researchers (e.g. Wallace and Foss 1995; Sreenivasan et al. 1977). While it is fraught with difficulties to measure the above two dissipation fields simultaneously, direct numerical simulations (DNS) complement experiments in some respects and provide new information on both statistical and structural aspects of the small-scale structures since they can resolve complete information on three-dimensional vorticity and full energy and temperature dissipation fields. The correlation of the above two dissipation fields can therefore be analyzed using DNS results (Wang et al. 1999). Differences of the correlations are compared when either the full expressions for ε and χ or their isotropic counterparts ε_{iso} and χ_{iso}, i.e.

$$\varepsilon_{iso}=15\nu u_{1,1}^2 \qquad (3)$$

and

$$\chi_{iso}=3\kappa\theta_{,1}^2 \qquad (4)$$

are used. The numerical study of Ruetsch and Maxey (1991) showed that intense ω^2 occurs in vorticity tubes and

ε is strongly correlated with these tubes. The regions where χ is the largest are dissociated from the vortex tubes and occur as large flat sheets. There is general agreement that the highest vorticity appears to reside in tubes while the moderate vorticity resides in sheets with large concentrations of strain rate and scalar gradient nearby. The moderate values of the energy dissipation rate surround the tubes while the large values of the scalar gradient are wrapped in sheets around the tubes and this gradient is in the direction of the compressive rate of strain. This suggests a relatively high correlation between ω^2 and ε but a poor correlation between χ and ω^2 or ε. Results obtained by simply approximating ε and χ by ε_{iso} and χ_{iso} [i.e. Eqs. (3) and (4)] based on isotropic assumption have yielded rather disparate values for the correlation between ε and χ (e.g. Antonia and Van Atta 1975; Meneveau et al. 1990).

The main objective of this paper is to measure the energy and temperature dissipation rates simultaneously in a cylinder wake using more reasonable approximations to ε and χ than ε_{iso} and χ_{iso}. On the basis of these measurements, the correlations between the two dissipation fields and the vorticity are further examined. The correlations between vorticity and temperature fluctuations are also analyzed.

EXPERIMENTAL DETAILS

The experiments were conducted in a wind tunnel with a cross-section of 400 mm × 400 mm and 2 m long. The free stream velocity U_∞ is about 3.6 m/s, corresponding to a Taylor microscale Reynolds number R_λ ($\equiv u_1'\lambda/\nu$, where $\lambda = u_1'/u_{1,1}'$ is the Taylor microscale and the prime denotes rms value) of about 40 (or $\mathrm{Re} = U_\infty d/\nu = 1520$, where $d \equiv 6.35$ mm is the diameter of the stainless steel cylinder). The measurement location is at $x_1/d = 240$. A probe consisting of four hot wires and a pair of parallel cold wires (Figure 1) was used to approximate the energy and temperature dissipation rates simultaneously. The four hot wires also allow the calculation of the spanwise component (ω_3) of the vorticity vector using the measured velocity signals u_1 and u_2. With the pair of parallel cold wires, two components, $\theta_{,1}$ and $\theta_{,2}$, of χ were measured simultaneously. The separation Δx_2 between the two parallel hot wires c and d and Δx_3 between the two inclined hot wires a and b are about 1.6 mm. The separation Δx_c between the two parallel cold wires is about 1.95 mm.

The hot and cold wires were etched from Wollaston (Pt-10%Rh) wires. The active lengths are about $200d_w$ and $800d_w$ for the hot and cold wires respectively (where d_w is the diameter of the wires and equals to 2.5 μm for the hot wires and 0.64 μm for the cold wires). The hot wires were operated with in-house constant temperature circuits at an overheat ratio of 0.5. The cold wires were operated with constant current (0.1 mA) circuits. The output signals from the anemometers were passed through buck and gain circuits and low-pass filtered at a frequency f_c of 800 Hz. The filtered signals were subsequently sampled at a frequency $f_s = 2f_c$ using a 16 bit A/D converter.

Using the present probe, the velocity derivatives $u_{1,1}$, $u_{1,2}$ and $u_{2,1}$ are measured simultaneously. Assuming local isotropy and homogeneity, simultaneous approximations to ε can be made using continuity (Zhou and Antonia 2000), viz.

$$\varepsilon_{ap} \approx \nu\left(6u_{1,1}^2 + 3u_{1,2}^2 + 2u_{2,1}^2 + 2u_{1,2}u_{2,1}\right) \qquad (5)$$

where the subscript *ap* represents "approximation". The two parallel cold wires are capable of measuring the temperature derivatives $\theta_{,1}$ and $\theta_{,2}$. The temperature dissipation rate χ can then be approximated as (Anselmet and Antonia 1985)

$$\chi_{ap} \approx \kappa\left(\theta_{,1}^2 + 2\theta_{,2}^2\right) \qquad (6)$$

Since more derivative correlations are included in Eq. (5) or (6), it is expected that they should provide more reasonable approximations to ε or χ than when ε_{iso} or χ_{iso} [Eqs. (3) or (4)] is used. With the present four hot-wire probe, the transverse vorticity component ω_3 can be obtained viz.

$$\omega_3 = u_{2,1} - u_{1,2} \approx \frac{\Delta u_2}{\Delta x_1} - \frac{\Delta u_1}{\Delta x_2} \qquad (7)$$

where Δu_1 in Eq. (7) is velocity difference between the longitudinal velocity fluctuations from the two parallel wires c and d. Δu_2 represents the difference between values of Δu_2 at the same point in space but separated by one sampling time interval $\Delta t (\equiv 1/f_s)$. In Eq. (7), Taylor's hypothesis, i.e. $\Delta\alpha/\Delta x_1 = -U_1^{-1}\Delta\alpha/\Delta t$ (α represents u_2), is used.

BASIC PERFORMANCE CHECK OF THE PROBE

Before presenting the statistics of ω_3, it is relevant to address the effect of imperfect spatial resolution of the probe has on the measurement of ω_3 and its components. The spectra of the velocity derivatives and the vorticity are attenuated due to the finite wire length and wire separation. This attenuation effect can be corrected based on the assumption of local isotropy. Details of the correction procedures can be found in Antonia et al. (1996).

In Figure 2, due to the spectral attenuation of the velocity derivatives, the directly measured values of ω_3' are underestimated by about 10% around the centerline region ($x_2/L \le 1$). They agree well ($\le 3\%$ in the region of $x_2/L = 1$) with the isotropic values ($\equiv 5 < u_{1,1}^2 >$) after correction near the centerline region. Both of the two data sets are about 10% smaller than those obtained by Antonia et al. (1988) and Zhu and Antonia (1999).

LOCAL ISOTROPY CHECKS

Since velocity derivatives give more weight to the high wavenumbers of the spectra than velocity fluctuations, theoretically, $u_{i,j}$ or ω_i should provide a better test for local isotropy than u_i. A measure of anisotropy is provided by comparing the measured spectrum of transverse or spanwise vorticity with that calculated based on isotropy.

For isotropic turbulence, the spectrum $\phi_{\omega_3}(k_1)$ can be calculated from $\phi_{u_{1,1}}$ (Kim and Antonia (1993)

$$\phi_{\omega_3}^{cal}(k_1)=\frac{5}{2}\phi_{u_{1,1}}(k_1)-\frac{k_1}{2}\frac{\partial\phi_{u_{1,1}}(k_1)}{\partial k_1}+2\int_{k_1}^{\infty}\frac{\phi_{u_{1,1}}(k_1)}{k}dk \quad (8)$$

The components of $\phi_{\omega_3}(k_1)$ can also be calculated using the isotropic relations:

$$\phi_{u_{2,1}}^{cal}(k_1)=\frac{3}{2}\phi_{u_{1,1}}-\frac{1}{2}k_1\frac{\partial\phi_{u_{1,1}}}{\partial k_1} \quad (9)$$

$$\phi_{u_{1,2}}^{cal}(k_1)=2\int_{k_1}^{\infty}\frac{\phi_{u_{1,1}}(k)}{k}dk \quad (10)$$

and

$$Co_{u_{2,1}u_{1,2}}^{cal}=-\frac{1}{2}\phi_{u_{1,1}}(k_1) \quad (11)$$

where $\phi_{u_{1,1}}$ is the streamwise velocity derivative spectrum. The measured spectra of ω_3 and its components are compared with the corresponding isotropic calculations in Figure 3. To account for the effect of spectral attenuation, all the spectra in the figure are corrected. While the measured spectrum $\phi_{u_{1,2}}$ agrees well with the isotropic distribution over the entire wavenumber range, the measured spectrum $\phi_{u_{2,1}}$ agrees well with the isotropic distribution only for $k_1^*>0.03$. This result seems to suggest that the transverse velocity derivatives are more related with small scale structures and therefore satisfy local isotropy at all wavenumbers even at low R_λ (≈ 40 in the present study). The measured cospectrum $-Co_{u_{2,1}u_{1,2}}(k_1)$ is also shown and compared with isotropic calculation in Figure 3. The measured distribution agrees reasonably well with the calculated one over the wavenumber range of $k_1^*=0.004\sim 0.4$. The upturn of the measured distributions at high wavenumbers may be due to noise contamination. All the results shown in Figure 3 imply that local isotropy is approximately satisfied on the centerline of the wake, even the Taylor microscale Reynolds number R_λ is low, reflecting the fact that vorticity dominate phenomena is mainly associated with the small-scale structures of turbulence. Same level of agreement between the measured temperature derivative spectra and isotropic calculations can also be obtained (results are not shown here). The departure of the measured temperature derivative spectra from isotropic calculations at the low wavenumber region is caused by low frequency noise contamination, reflected by the low signal-to-noise ratio ($\approx$70) in the experiment.

To check the departure of the measured vorticity spectra from local isotropy in a more systematic way, Figure 4 compares the ratio $\phi_{\omega_3}^{cal}/\phi_{\omega_3}^{m}$ at different transverse locations. When local isotropy is perfectly satisfied, this ratio should be equal to 1, as the solid horizontal line shown in Figure 4. The ratio $\phi_{\omega_3}^{cal}/\phi_{\omega_3}^{m}$ on the centerline is close to 1 (within $\pm 5\%$) over the whole wavenumber range, independently of the small value of R_λ in the present study. This ratio is relatively small (0.87) only for $k_1^*>0.02$ when x_2/L increases to 1.2, indicating slight departure from isotropy. The departure of the measured spectrum from the isotropic calculation is more apparent at $x_2/L=1.5$, where only the small scale structures, e.g. $k_1^*>0.1$, satisfy isotropy. This value increases to $k_1^*>0.65$ at the edge of the wake ($x_2/L=2$). The results shown in Figure 4 indicate that local isotropy is valid only in the range of $x_2/L\le 1.2$.

CORRELATIONS BETWEEN ENERGY AND TEMPERATURE DISSIPATION RATES

To check of the validity of Eqs. (5) and (6) in the spectral domain, Figures 5(a,b) show the spectra corresponding to energy and temperature dissipation rates obtained using different methods. The spectrum $\phi_{\varepsilon_f}(k_1)$ is obtained using a four-X-wire probe (Zhu and Antonia 1999), by which 9 of the 12 velocity derivative correlations involved in ε can be measured simultaneously. Since the spectra are normalized by the Kolmogorov scales, the areas under the various distributions should be equal to 1. By integrating under the distributions of the spectra over the range of $k_1^*=0-\infty$, the areas are close to 1 ($\pm 5\%$). While the distribution of $\phi_{\varepsilon_{ap}}(k_1)$ agrees well with that of $\phi_{\varepsilon_f}(k_1)$ at all wavenumbers as indicated in Figure 5a, $\phi_{\varepsilon_{iso}}(k_1)$ departs significantly from both $\phi_{\varepsilon_f}(k_1)$ and $\phi_{\varepsilon_{ap}}(k_1)$, except for $k_1^*>0.5$. This result indicates that the use of ε_{iso} as a substitute of ε, as usually used in experimental studies may cause significant errors, at least in the spectral domain. There is nearly no difference between the spectra $\phi_{\chi_f}(k_1)$ $[\equiv\phi_{\theta_{,1}}(k_1)+\phi_{\theta_{,2}}(k_1)+\phi_{\theta_{,3}}(k_1)]$ and $\phi_{\chi_{ap}}(k_1)$ $[\equiv\phi_{\theta_{,1}}(k_1)+2\phi_{\theta_{,2}}(k_1)]$ as demonstrated in Figure 5b. This is mainly because of the good agreement between the measured distributions $\phi_{\theta_{,2}}(k_1)$ and $\phi_{\theta_{,3}}(k_1)$. The measured distribution $\phi_{\chi_{iso}}(k_1)$ departs significantly from both $\phi_{\chi_f}(k_1)$ and $\phi_{\chi_{ap}}(k_1)$ over the whole wavenumber range, indicating the inappropriateness of χ_{iso} as a substitute of χ, at least in the spectral domain.

The correlation between $\ln\varepsilon_r$ and $\ln\chi_r$ is important in quantifying the behavior of the temperature structure function $<(\delta\theta)^n>$ in the inertial range. Van Atta (1971) noted that $\rho_{\ln\varepsilon_r,\ln\chi_r}$ should vary only weakly with r across the inertial range. In the present study, an inertial range is not expected due to the low R_λ. A scaling range, instead, centered on the value of r^* at which $<\left|\delta u_1^*\right|^3>r^{*-1}$ is maximum, can be defined, where $\delta u_1\equiv u_1(x+r)-u_1(x)$ is the velocity increment between two points separated by a distance r. The values of $\rho_{\ln\varepsilon_r,\ln\chi_r}$ calculated using either

$(\varepsilon_{ap}, \chi_{ap})$ or $(\varepsilon_{iso}, \chi_{iso})$ in the present wake flow are shown in Figure 6. The magnitude of $\rho_{\ln\varepsilon_r, \ln\chi_r}$ obtained using $(\varepsilon_{ap}, \chi_{ap})$ is about 20% larger in the scaling range $10 \le r^* \le 40$ than when $(\varepsilon_{iso}, \chi_{iso})$ are used. This finding suggests that for this flow, the isotropic surrogates $(\varepsilon_{iso}, \chi_{iso})$ cannot represent (ε, χ) properly. The magnitude of $\rho_{\ln\varepsilon_r, \ln\chi_r}$ in the present wake is about twice as large as that in the grid flow (Mydlarski and Warhaft 1998, $R_\lambda = 582$), where $(\varepsilon_{iso}, \chi_{iso})$ were used to represent (ε, χ). It is also larger than that reported by Meneveau et al. (1990) in a heated wake at higher values of R_λ. This result may suggest that the correlation coefficient $\rho_{\ln\varepsilon_r, \ln\chi_r}$ decreases with the increase of R_λ in the same flow, which is in contrast with the R_λ dependence of $\rho_{\ln\varepsilon_r, \ln\chi_r}$ indicated by the DNS data of Wang et al. (1999) in forced box turbulence. The present measured values of $\rho_{\ln\varepsilon_r, \ln\chi_r}$ differ significantly from those for a heated turbulent jet (Antonia and Van Atta 1975) and the atmospheric surface layer (Antonia and Chambers 1980). Meneveau et al. (1990) noted that the apparent discrepancy of $\rho_{\ln\varepsilon_r, \ln\chi_r}$ may be due to the influence of the hot wire on the cold wire signals; this effect may be significant in a turbulent jet because of the high turbulent intensity of this flow. However, this explanation may not be adequate, especially when the separation between the hot and cold wires is sufficient to avoid any interference from the hot wire signals. The large discrepancy in Figure 6 suggests that the magnitude of $\rho_{\ln\varepsilon_r, \ln\chi_r}$ may depend on the relations used to approximate ε and χ. A more likely possibility is the effect of R_λ. Further, the dependence of $\rho_{\ln\varepsilon_r, \ln\chi_r}$ on the nature of the flow or the initial conditions cannot be dismissed.

The correlations between ω_3^2, ε and ε can be quantified by examining $<\beta|_\alpha>$, the expectations of β conditioned on particular values of α (where α and β represent ω_3^2, ε and χ). This conditional expectation is defined as:

$$<\beta|_\alpha> = \int_{-\infty}^{\infty} \beta p(\beta|_\alpha) d\beta \qquad (12)$$

where $p(\beta|_\alpha) \equiv p_{\alpha,\beta} / p_\alpha$ is the pdf of β conditioned on α. The expectations of ε_{ap} and χ_{ap} conditioned on ω_3^2, normalized by their mean values, are shown in Figure 7. The values $<\varepsilon_{ap}|_{\omega_3^2}> / <\varepsilon_{ap}>$ increase linearly as ω_3^2 increases with a gradient of 0.9, reflecting a strong dependence of ε_{ap} on ω_3^2. The dependence of $<\varepsilon_{ap}>$ on $<\omega_3^2>$, as shown in Figure 7, is consistent with that reported by Wang et al. (1999) using direct numerical simulations. The values of $<\chi_{ap}|_{\omega_3^2}> / <\chi_{ap}>$ increase slowly with $\omega_3^2 / (\omega_3^2)'$ (with a gradient close to 0.3) when the later is smaller than 0.6, indicating a small correlation between χ and ω_3^2. When $\omega_3^2 / (\omega_3^2)'$ is larger than 0.6, $<\chi_{ap}|_{\omega_3^2}> / <\chi_{ap}>$ keeps approximately constant with a magnitude close to 1.1. This result indicates that there is nearly no correlation between χ and ω_3^2 for large fluctuations.

The correlation coefficients between vorticity and temperature fluctuations have been calculated for various combinations. The correlation coefficient $\rho_{\alpha,\beta}$ is defined in Eq. (2). Symmetry with respective to the x_3-direction requires that the correlation between θ and ω_2 be zero (where ω_2 is the transverse vorticity component and can be measured by rotating the probe shown in Fig.1 by 90°). This is the case as shown in Figure 8 from the measured values. The correlation coefficient between θ and ω_3 has negative values for $x_2 / L > 0$. The largest negative values occur near the edge of the wake. The negative values of ρ_{θ,ω_3} in the upper part of the wake indicate that spanwise vorticity mainly resides in relatively warm fluid moving towards the wake edge. This is consistent with negative mean temperature gradient in this region. Observations of dye in the far wake of a cylinder (Antonia et al. 1987) suggested a reasonable high correlation between dye concentrations in the outer wake and spanwise vorticity, as inferred from the path of dye streaklines introduced outside the edge of the wake.

CONCLUSIONS

A six-wire probe has been used to approximate energy and temperature dissipation rates in the far field of a cylinder wake. The performance of the probe has been tested satisfactorily. The departure from local isotropy was checked by examining the ratio $\phi_{\omega_3}^{cal} / \phi_{\omega_3}^{m}$ at different transverse locations. It is found that for $x_2 / L \le 1.2$, the ratio is quite close to 1, indicating the satisfactory of local isotropy in this region. When x_2 / L further increases, the departure of the ratios from 1 becomes apparent at low wavenumbers. This result is consistent with the fact that at the outer region of the wake, local isotropy will become invalid due to the influence of large-scale turbulence structures. Previous experimental results obtained using ε_{iso} and χ_{iso} yields rather disparate values for $\rho_{\ln\varepsilon_r, \ln\chi_r}$ in different flows and at different Reynolds numbers. The large scatter of $\rho_{\ln\varepsilon_r, \ln\chi_r}$ indicates that this correlation coefficient may also depend on the magnitude of R_λ as well as the nature or the initial conditions of the flow. The correlation between ε_{ap} and ω_3^2 is found much higher than that between χ_{ap} and ω_3^2, in accordance with DNS-based investigations. The negative values of ρ_{θ,ω_3} in the upper part of the wake indicate that spanwise vorticity mainly resides in the relatively warm fluids near the wake edge. This is also consistent with the negative mean temperature gradient in this region.

ACKNOWLEDGEMENTS

The financial support from Mindef-NTU joint project is gratefully acknowledged.

REFERENCES

Anselmet F. and Antonia, R. A., 1985, "Joint statistics between temperature and its dissipation in a turbulent jet", *Phys Fluids,* 28, pp. 1048-1051.

Antonia, R. A., Browne, L. W. B. and Fulachier, L., 1987, "Average wavelength of organised structures in the turbulent far wake of a cylinder", *Exp in Fluids,* 5, pp. 298-304.

Antonia, R. A., Browne, L. W. B. and Shah, D. A., 1988, "Characteristics of vorticity fluctuations in a turbulent wake", *J Fluid Mech,* 189, pp. 349-365.

Antonia, R. A. and Chambers, A. J., 1980, "Velocity and temperature derivatives in the atmospheric surface layer", *Boundary-Layer Meteorol,* 18, pp. 399-410.

Antonia, R. A., Zhu, Y. and Shafi, H. S., 1996, "Lateral vorticity measurements in a turbulent wake", *J Fluid Mech,* 323, pp. 173-200.

Antonia, R. A. and Van Atta, C. W., 1975, "On the correlation between temperature and velocity dissipation fields in a heated turbulent jet", *J Fluid Mech,* 67, pp. 273-287.

Kim, J. and Antonia, R. A., 1993, "Isotropy of the small-scales of turbulence at low Reynolds number", *J Fluid Mech,* 251, pp. 219–238.

Meneveau, C., Sreenivasan, K. R., Kailasnath, P. and Fan, M., 1990, "Joint multifractal measures: theory and applications to turbulence", *Phys Rev A,* 41, pp. 894-913.

Mydlarski, L. and Warhaft, Z., 1998, "Passive scalar statistics in high-Peclet-number grid turbulence", *J Fluid Mech,* 358, pp. 135–175.

Ruetsch, G. R. and Maxey, M. R., 1991, "Small-scale features of vorticity and passive scalar fields in homogenous isotropic turbulence", *Phys Fluids A,* 3, pp. 1587-1597.

Sreenivasan, K. R., Antonia, R. A. and Danh, H. Q., 1977, "Temperature dissipation fluctuations in a turbulent boundary layer", *Phys Fluids,* 20, pp. 1238-1249.

Stolovitzky, G., Kailasnath, P. and Sreenivasan, K. R., 1995, "Refined similarity hypotheses for passive scalars mixed by turbulence", *J Fluid Mech,* 297, pp. 275-291.

Van Atta, C. W., 1971, "Influence of fluctuations in local dissipation rates on turbulent scalar characteristics in the inertial subrange", *Phys Fluids,* 14, pp. 1803-1815.

Wallace, J. M. and Foss, J. F., 1995, "The measurement of vorticity in turbulent flows", *Ann Rev Fluid Mech,* 27, pp. 469-514.

Wang, L. P., Chen, S. and Brasseur, J. G., 1999, "Examination of hypotheses in Kolmogorov refined turbulence theory through high-resolution simulations, Part 2. Passive Scalar Field", *J Fluid Mech,* 400, pp. 163-197.

Zhou, T. and Antonia, R. A., 2000, "Approximation for turbulent energy and temperature dissipation rates in grid turbulence", *Phys Fluids,* 12, pp. 335-344.

Zhu, Y. and Antonia, R.A., 1999, "Performance of three-component vorticity probe in a turbulent far-wake", *Exp in Fluids,* 27, pp. 21-30.

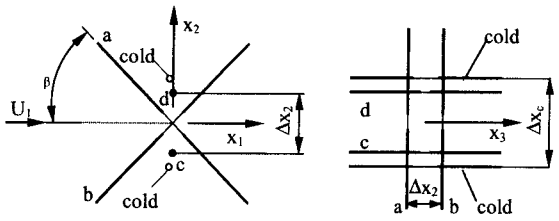

(a) Side View (b) Front View

Figure 1. Sketches of the 6-wire probe. (a) Side view; (b) Front view.

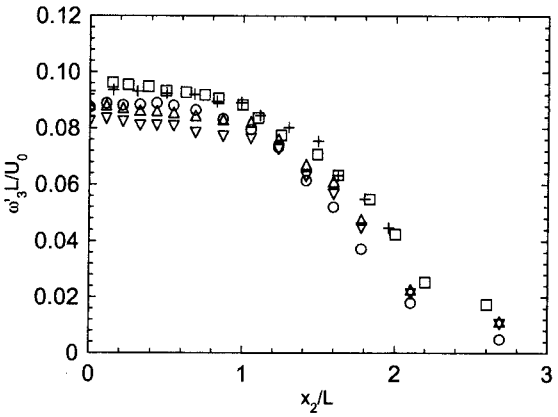

Figure 2. Distributions of rms values of ω_3. ∇, present measurement (uncorrected); Δ, present measurement (corrected). +, Antonia et al. (1988); , Zhu and Antonia (1999). O, isotropic values ($5 < u_{1,1}^2 >$).

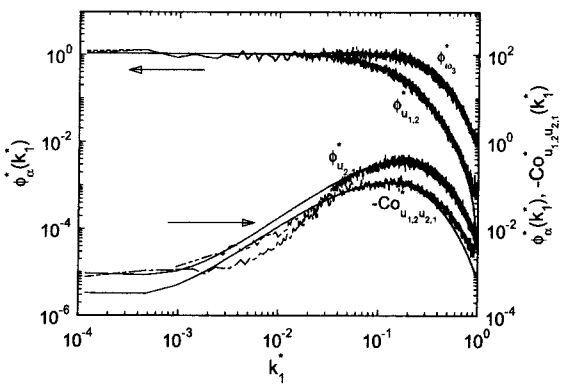

Figure 3. Comparison of measured spanwise vorticity spectrum and its components with isotropy on the centerline of the wake. —, isotropic calculations; ---, $\phi^m_{\omega_3}$; – – , $\phi^m_{u_{1,2}}$; – - –, $\phi^m_{u_{2,1}}$; – - - -, $-Co^m_{u_{1,2}u_{2,1}}$.

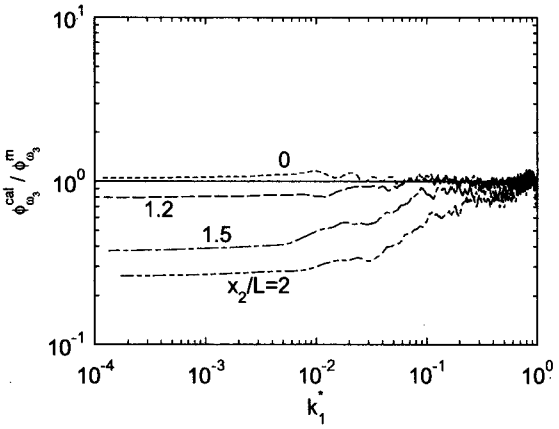

Figure 4. Ratios of the calculated and measured spectra of ω_3 at different transverse locations.
---, $x_2/L=0$; – – –, $x_2/L=1.2$; – – –, $x_2/L=1.5$; – – –, $x_2/L=2$. The horizontal line indicates the isotropic value of 1.

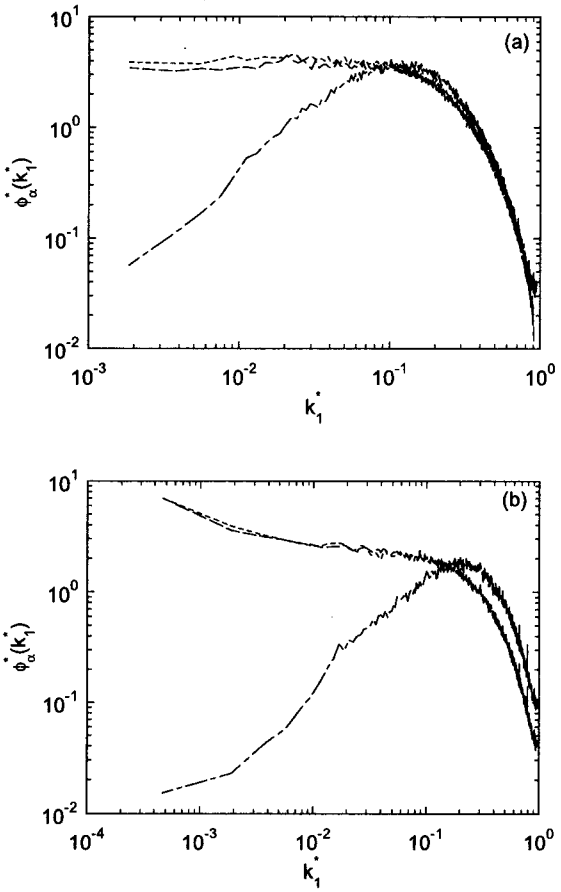

Figure 5. Spectra of energy and temperature dissipation rates obtained using various methods. (a) ϕ_ε; (b) ϕ_χ.
---, ϕ_{ε_f} (or ϕ_{χ_f}); — —, $\phi_{\varepsilon_{ap}}$ (or $\phi_{\chi_{ap}}$); — - —, $\phi_{\varepsilon_{iso}}$ (or $\phi_{\chi_{iso}}$).

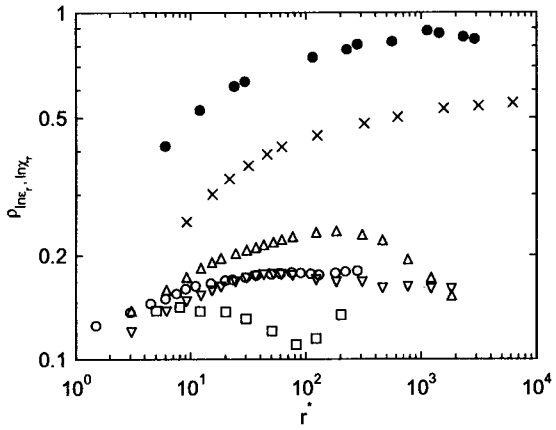

Figure 6. Comparison of correlation coefficient $\rho_{\ln\varepsilon_r,\ln\chi_r}$ with previous experimental values.
Present: Δ, $\varepsilon=\varepsilon_{ap}$, $\chi=\chi_{ap}$; ∇, $\varepsilon=\varepsilon_{iso}$, $\chi=\chi_{iso}$. , Meneveau et al. (1990); •, Antonia and Van Atta (1975); ×, Antonia and Chambers (1980); O, Wang et al. (1999).

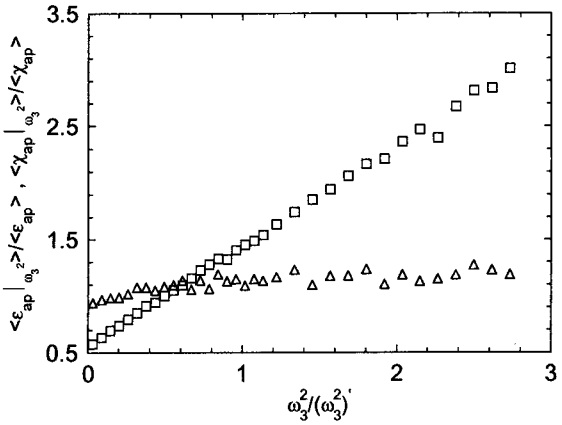

Figure 7. Expectations of ε_{ap} and χ_{ap} conditioned on particular values of ω_3^2. , ε_{ap}; Δ, χ_{ap}.

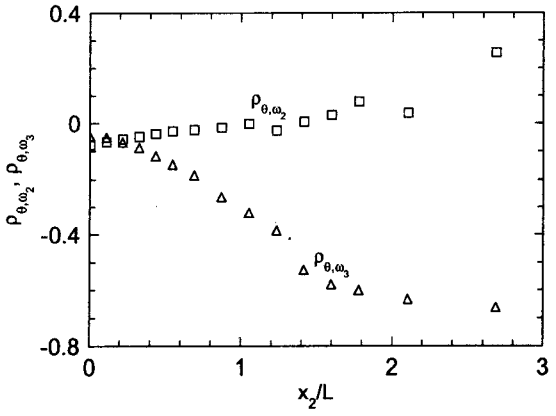

Figure 8. Correlation coefficients between θ and ω_2, θ and ω_3. , ρ_{θ,ω_2}; Δ, ρ_{θ,ω_3}.